



HAL
open science

First-principles investigation on multiferroic properties of BiFeO₃-REMnO₃ (RE = Er, Eu, Gd, Ho, La, Tb)

Abdelilah Benyoussef, Abdallah El Kenz, Abdelilah Lahmar, Mohamed Ait Tamerd, Majid El Kassaoui, Brahim Abraime, Adil Marjaoui, Mimoun El Marssi

► To cite this version:

Abdelilah Benyoussef, Abdallah El Kenz, Abdelilah Lahmar, Mohamed Ait Tamerd, Majid El Kassaoui, et al.. First-principles investigation on multiferroic properties of BiFeO₃-REMnO₃ (RE = Er, Eu, Gd, Ho, La, Tb). *Materials Today Communications*, 2021, 29, 10.1016/j.mtcomm.2021.102976 . hal-03627365

HAL Id: hal-03627365

<https://u-picardie.hal.science/hal-03627365>

Submitted on 5 Jan 2024

HAL is a multi-disciplinary open access archive for the deposit and dissemination of scientific research documents, whether they are published or not. The documents may come from teaching and research institutions in France or abroad, or from public or private research centers.

L'archive ouverte pluridisciplinaire **HAL**, est destinée au dépôt et à la diffusion de documents scientifiques de niveau recherche, publiés ou non, émanant des établissements d'enseignement et de recherche français ou étrangers, des laboratoires publics ou privés.



Distributed under a Creative Commons Attribution - NonCommercial 4.0 International License

First-principles investigation on multiferroic properties of BiFeO₃-REMnO₃ (RE = Er, Eu, Gd, Ho, La, Tb)

Mohamed Ait Tamerd^{a,b,*}, Majid El Kassaoui^b, Brahim Abraime^b, Adil Marjaoui^c, Mimoun El Marssi^a, Abdeilah Benyoussef^{b,d}, Abdallah El Kenz^b, Abdelilah Lahmar^a.

^aLaboratoire de Physique de La Matière Condensée (LPMC), Université de Picardie, Amiens, France.

^bLaMCScl (PPR15), Faculty of Science, Mohammed V University, Rabat, Morocco

^cGroup of Thin films and nanomaterials, UAE/U01FST, Faculty of Sciences and Techniques of Tangier, Abdelmalek Essaadi University, Tangier 90000, Morocco

^dHassan II Academy of Science and Technology, Rabat, Morocco.

*Corresponding authors: aittamerd@gmail.com

Abstract:

Structural and multiferroic properties of BiFeO₃-REMnO₃ solid solution (RE = Er, Eu, Gd, Ho, La, Tb) have been investigated using the first-principle calculations. Simultaneous substitution of Gd and Mn in BiFeO₃ of 12.5 % has been carried out. We found that the total magnetic moment in BiFeO₃-REMnO₃ is decisively governed by the magnetic moments of rare-earth elements. Our calculations achieved a total magnetic moment of 3.58, 4.69, 5.8, 4.27, 1.5 and 6.31 μ_B in BiFeO₃-REMnO₃ for RE= Er, Eu, Gd, Ho, La and Tb, respectively. The calculated total densities of states for all studied materials are clearly asymmetrical with metal characteristics. Further, a pseudo Jahn–Teller distortion was predicted for BiFeO₃-GdMnO₃ with the changes in the octahedral tilting angle θ which is responsible for higher magnetization in this system. The spontaneous polarization of BiFeO₃-REMnO₃ systems was determined by berry phase methods. The obtained results are close to the experimental and other theoretical results.

Keyword: *multiferroic properties; first-principle calculations; density of states; spontaneous polarization; magnetic moments; pseudo Jahn–Teller.*

1. Introduction:

As a promising multiferroic material, perovskite BiFeO₃, which shows the coexistence of both ferroelectricity and antiferromagnetic orders, is a very interesting system, due to their possible technological applications, such as electric random access memories (FeRAMs) [1,2], potential magnetoelectrics, spintronics, [3-5] because its room-temperature multiferroic

properties [6-8]. In the bulk form, BiFeO₃ exhibits a rhombohedral distorted perovskite structure with the space group of *R3c* [9], reported with a large remnant polarization of ~90 $\mu\text{C cm}^{-2}$ [10]. Further, this compound is a G-type antiferromagnetic with a Neel temperature $T_N = 643 \text{ K}$ [11] and ferroelectric with a Curie temperature $T_C = 1103 \text{ K}$ [12].

Recently, intense experimental and theoretical research investigations have been focused on the effects of simultaneous substitution of Bi- and Fe- sites in BiFeO₃ to improve its multiferroic properties for multifunctional applications. M.A. Basith et al [13,14] reported that the dielectric and magnetic properties of BiFeO₃ have been improved by co-substitution of Bi- and Fe- sites of BiFeO₃ by ions such as Gd and Ti. Further, Tang et al [15] showed that the ferroelectric properties were enhanced in Bi_{0.9}Gd_{0.1}Fe_{0.9}Mn_{0.1}O₃ in comparison with BiFeO₃. In addition, Zhou et al. surmised that saturation magnetization and optical band gap increases in Sm and Mn co-doped BiFeO₃ [16]. In the other hand, a structural transformation from rhombohedral (*R3c*) to orthorhombic (*Pn21a*) symmetry with significantly enhanced magnetization was obtained in BiFeO₃ co-substituted with Gd and Mn [17]. Similar improvement of multiferroic properties was observed by Lahmar et al [18,19] for rare earth element (RE) and Mn co-substitution of BiFeO₃, where a structural transition from monoclinic (BiFeO₃) to orthorhombic (BiFeO₃-REMnO₃) was highlighted up to 10 mol% substitution concentration.

In the present work, spontaneous polarization, magnetic, and electronic properties of RE- and Mn- co- substituted BiFeO₃ were investigated by first principles. Furthermore, a pseudo Jahn–Teller distortion was predicted for the BiFeO₃-GdMnO₃ system. To the best of our knowledge, the first-principles study of RE- and Mn- co-substituted BiFeO₃ has not been reported yet. Thus, these results are likely to offer useful information to the research communities' deal with BFO based multiferroic materials.

2. Computational methods:

Density functional theory (DFT) [20,21] calculations were performed within the local spin density approximation (LSDA+U) as implemented in the ABINIT package [22]. We include an effective Hubbard parameter $U_{\text{eff}}=U-J$ equal to 4.5 eV, which is sufficient to describe related bulk properties and is a better description of localized Fe(3d) and Mn(3d) electron [23]. While for rare earth 4f-orbitals, the U_{eff} is fixed in about 8 eV [24]. We use optimized pseudo-potentials generated with OPIUM [25,26]. These calculations are

performed with a kinetic energy cutoff of 50 Hartree, a $10 \times 8 \times 10$ Monkhorst-Pack k-point mesh and Gaussian smearing of 0.04 eV. Spin-polarized calculations with a G-type antiferromagnetic order have been performed for $\text{BiFeO}_3\text{-REMnO}_3$. In our calculation, the spin-orbit interaction is not included.

3. Results and discussion

3.1. Stability and structural analysis:

It was reported that the $\text{BiFeO}_3\text{-GdMnO}_3$ crystalized under orthorhombic (Pn21a) with lattice parameters: $a=5.587 \text{ \AA}$, $b=7.7987 \text{ \AA}$ and $c=5.451 \text{ \AA}$ [17]. Likewise, Lahmar et al [19] observed that the structure of BiFeO_3 was adapted to the structure of rare-earth manganites REMnO_3 by adding 10 mol%. Herein, the co-substitution of BiFeO_3 with 12.5 % of RE and Mn were created by replacing Bi and Fe atoms by RE and Mn atoms in BiFeO_3 , respectively. In our calculations, four inequivalent configurations with different distributions of RE and Mn cations in the $2 \times 1 \times 1$ supercell have been considered as shown in **Figure.1**. Then, we optimized both the lattice parameters and the atomic positions of the $\text{BiFeO}_3\text{-REMnO}_3$ structure to obtain their ground state properties by minimization of the total energy, **Table 1** summarized the calculated total energies of $\text{BiFeO}_3\text{-REMnO}_3$ for the considered configurations. It was found that the configuration (3) is more stable for RE = Gd, Ho, La and Tb in $\text{BiFeO}_3\text{-REMnO}_3$, configuration (2) for $\text{BiFeO}_3\text{-ErMnO}_3$ and configuration (1) for $\text{BiFeO}_3\text{-EuMnO}_3$.

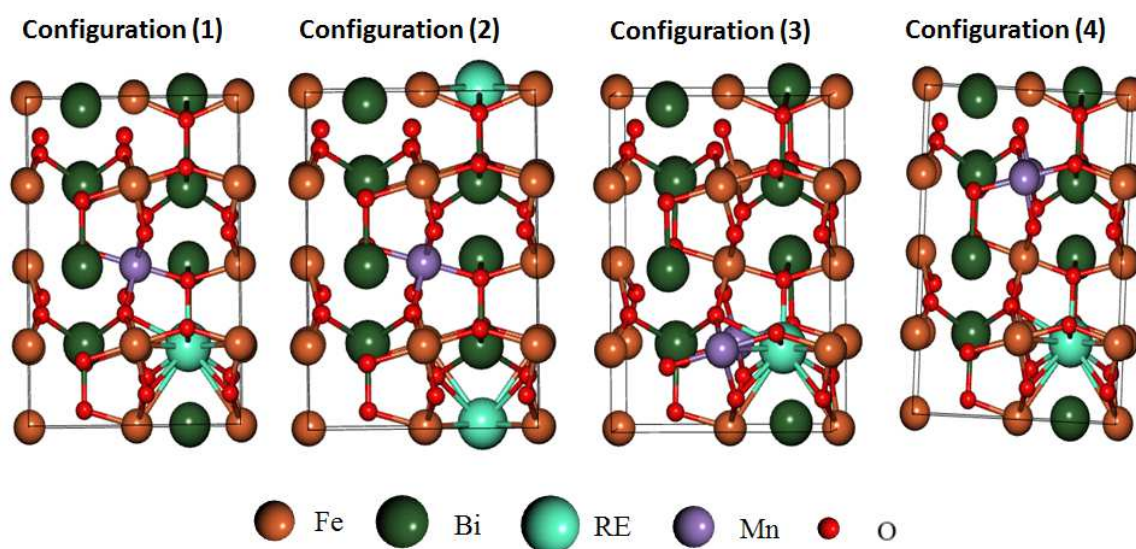


Figure 1: structure of $\text{BiFeO}_3\text{-REMnO}_3$ (RE=Er, Eu, Gd, Ho, La, Tb) with different configurations.

Table 1: The calculated total energies of $\text{BiFeO}_3\text{-REMnO}_3$ for the considered configurations.

$\text{BiFeO}_3\text{-REMnO}_3$	Configuration (1)	Configuration (2)	Configuration (3)	Configuration (4)
RE = Er	-1627.4478122	-1627.4478181	-1627.4291556	-1627.4261075
RE = Eu	-1497.2557803	-1497.2500953	-1497.2552961	-1497.2530702
RE = Gd	-2124.4348626	-2124.4348626	-2124.4383417	-2124.4353313
RE = Ho	-1599.8917145	-1599.8917145	-1599.8972722	-1599.8828313
RE = La	-1901.9595576	-1901.9595571	-1901.9597952	-1901.9596332
RE = Tb	-1552.6880289	-1552.6877883	-1552.6892636	-1552.6877660

Table 2 summarizes the optimized lattice parameters of $\text{BiFeO}_3\text{-REMnO}_3$ for different rare earth elements (RE = Er, Eu, Gd, Ho, La, Tb). The lattice parameters calculated are compared to the available experimental results. We note that the calculated lattice parameters for RE = Gd are close to the experimental results obtained by M. Hasan et al [17], with the observation of a structural transformation from rhombohedral (R3c) to orthorhombic (Pn21a) symmetry in co-substitution with Gd and Mn in BiFeO_3 .

Table 2: The calculated lattice parameters of $\text{BiFeO}_3\text{-REMnO}_3$. The experimental values are taken from Ref [17].

	a (Å)	b (Å)	c(Å)
$\text{BiFeO}_3\text{-ErMnO}_3$	10.476	14.435	10.211
$\text{BiFeO}_3\text{-EuMnO}_3$	10.394	14.516	10.191
$\text{BiFeO}_3\text{-GdMnO}_3$	10.355	14.410	10.113
Exp : Ref [17]	10.56	14.72	10.30
$\text{BiFeO}_3\text{-HoMnO}_3$	10.385	14.475	10.170
$\text{BiFeO}_3\text{-LaMnO}_3$	10.388	14.608	10.253
$\text{BiFeO}_3\text{-TbMnO}_3$	10.391	14.449	10.176

3.2. Electronic and magnetic properties

Figure.2a illustrates the total density of states of $\text{BiFeO}_3\text{-REMnO}_3$ (RE = Er, Eu, Gd, Ho, La, Tb). The vertical dashed lines denote Fermi energy level, which is indicated at 0 eV. Our calculations show that the $\text{BiFeO}_3\text{-LaMnO}_3$ has a symmetrical density of states. As a result, a minimum magnetic moment per cell of $1.5 \mu_B$ (see **Figure.2b**) and metallic behavior were observed for $\text{BiFeO}_3\text{-LaMnO}_3$. While, the asymmetrical total density of states with metal characteristics are observed for $\text{BiFeO}_3\text{-REMnO}_3$ with RE = Er, Eu, Ho, Gd and Tb.

Figure.2b shows the total and partial magnetic moments in BiFeO₃-REMnO₃. We note that the total magnetic moment is decisively governed by the magnetic moments of rare-earth elements. Our calculations achieved a total magnetic moment of 3.58, 4.69, 5.8, 4.27, 1.5 and 6.31 μ_B in BiFeO₃-REMnO₃ for RE= Er, Eu, Gd, Ho, La and Tb, respectively. It is worth noting that these results are similar to the observations reported on RE doped BiRE_{0.8}Fe_{0.9}Co_{0.1}O₃ (RE=La and Er) studied by first-principles [27]. Experimentally, W. Ye et al [28] reported that (Ho, Mn) co-doped BiFeO₃ thin films enhanced the basic magnetization. Moreover, this observation is in agreement with the results reported in refs [18,19], where the improvement of the multiferroic properties are related to the RE- and Mn-co-substituted BiFeO₃.

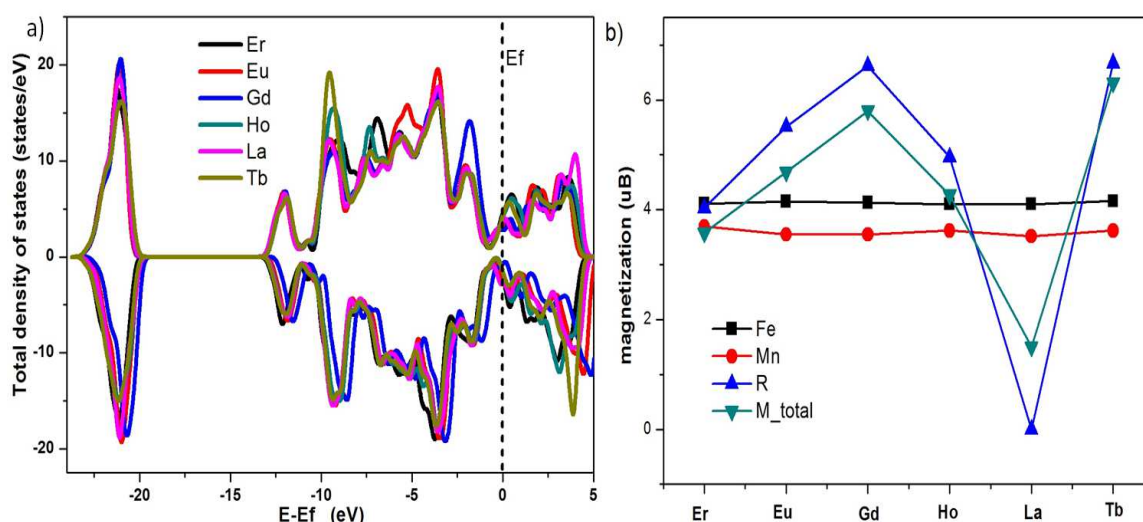
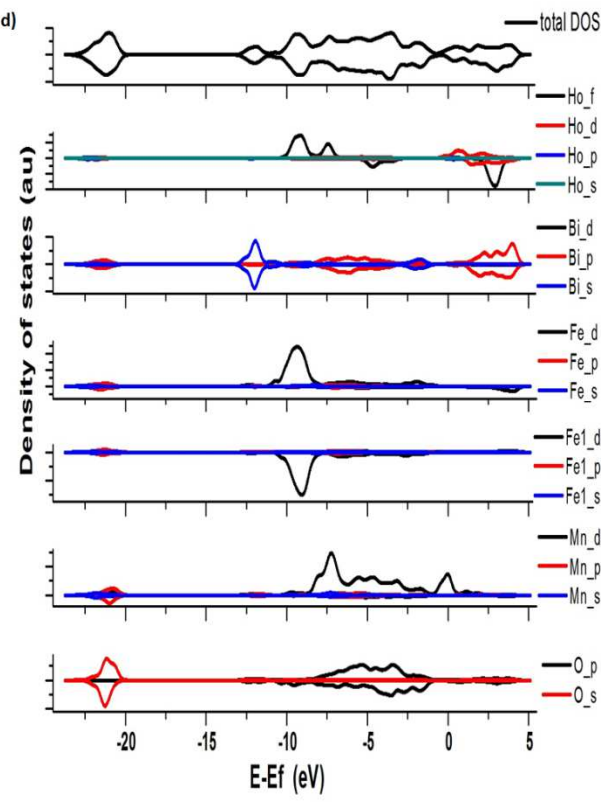
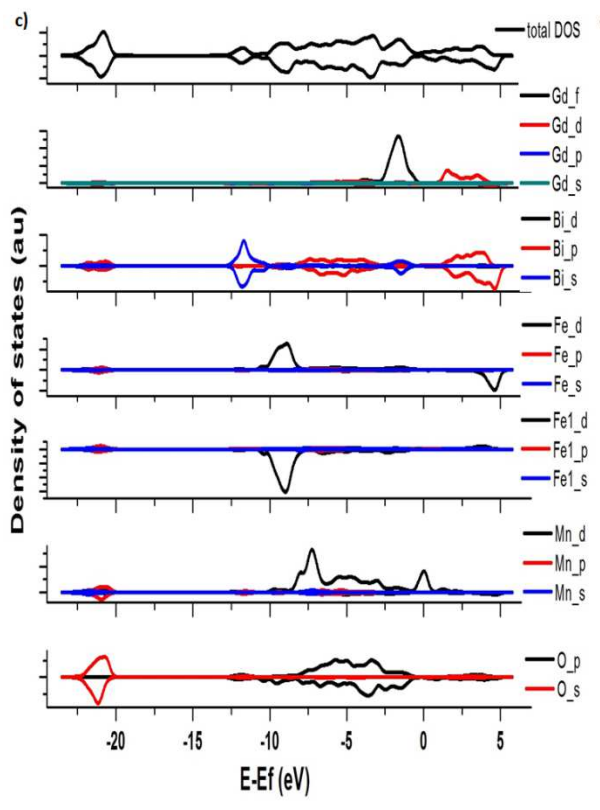
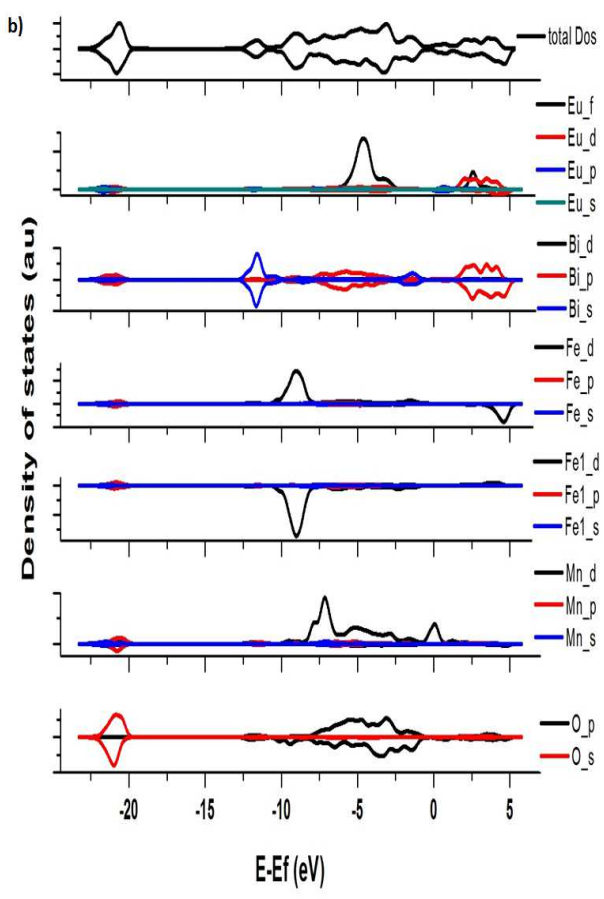
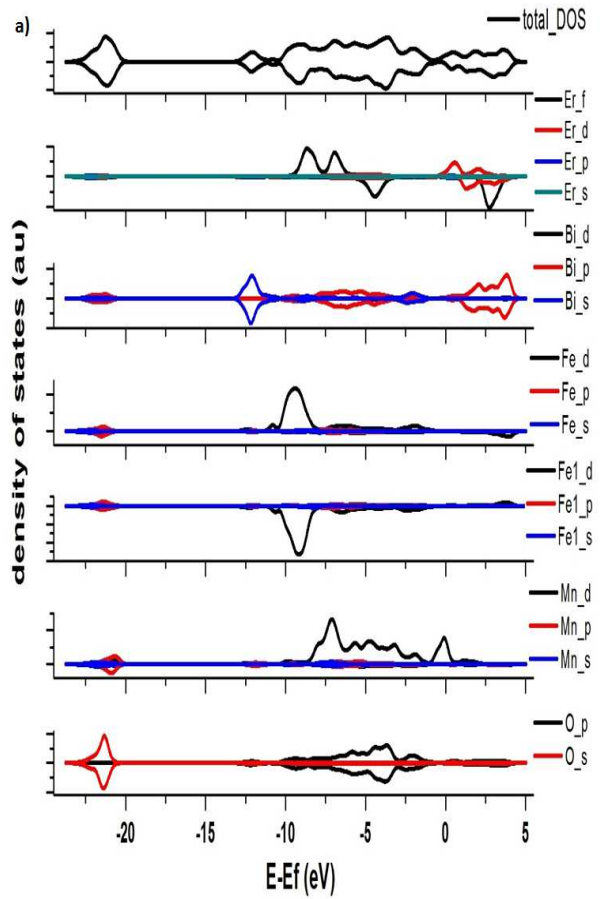


Figure.2: (a) Total density of states and (b) magnetic moments of BiFeO₃-REMnO₃ (RE = Er, Eu, Gd, Ho, La, Tb), the Fermi energy is set to be 0 eV.

The spin-up of the Er-4f state is presented from -9 to -2.5 eV which is hybridized with the Mn-3d, Bi-6p, Fe-3d and O-2p states as shown in **Figure.3a**. In addition, the conduction band minimum is principally among the contribution of the strong hybridizations of Er-4f, Er-5p and Bi-6p states. Experimentally, the magnetization improved in Bi_{0.8}Er_{0.2}Fe_{0.9}Mn_{0.1}O₃ compounds [29], due to the super-exchange interaction between Er-4f and Fe-3d electrons [30]. The density of states of BiFeO₃-EuMnO₃ is illustrated in **Figure.3b**. The valence band between -6 to 2.5 eV, is formed by states of Eu-4f, Mn-3d, Bi-6p, and O-2p atoms. The top of the conduction band is mainly formed by Eu-4f, Eu-4d, Fe-4d and Bi-6p. For BiFeO₃-GdMnO₃, the spin-up of Gd-4f localized in top of the valence band between 2.5 and 0 eV, which is hybridized with the O-2p state with a small contribution of Mn-d and Bi-s (see **Figure.3c**).

Similar behavior has been observed for $\text{BiFeO}_3\text{-HoMnO}_3$, where the Ho-4f states hybridized in valence band with the Mn-3d, Bi-6p, Fe-3d and O-2p states as shown in **Figure.3d**. Further, the Fermi level is occupied by the Ho-4d Mn-3d and O-2p states, suggesting that the incorporation of Ho and Mn changed the BiFeO_3 from a semiconductor to a conductor material. The maximum valence band is composed of Bi-6p, O-2p, Mn-3d and La-4d states with a strong overlapping between -7.5 eV and 0 eV as shows in **Figure.3e**. However, Spin-up of the Fe-3d state and spin down of Fe1-3d are localized at -9 eV, which is hybridized with the O-2p state. In addition, the lowest conduction band is composed of Bi-6p, Fe-3d, La-4d and La-5p states with a small admixture of O-2p states. Moreover, the partial density of states of $\text{BiFeO}_3\text{-TbMnO}_3$ is presented in **Figure.3f**. The valence band maximum is dominated by the Mn-3d, Bi-4d and O-2p states. The main Tb-4f valence band is found at around -9 eV, which hybridized with the Fe-3d and small contribution of Mn-3d and O-2p states. In addition, it is found that the unoccupied Tb-4f states are around 4 eV above the Fermi level. It can also be observed that in all $\text{BiFeO}_3\text{-REMnO}_3$ there is a sharp peak that appears at the Fermi level and it is half occupied with the spin-up of Mn-3d. Densities of states in $\text{BiFeO}_3\text{-REMnO}_3$ indicate that the strong hybridization of RE-4f, Mn-3d, Bi-6p, Fe-3d and O-2p states could be the electronic origin of magnetoelectric coupling in this system. It was reported that in pure BiCoO_3 hybridizations between Bi-O and Co-O play important roles in the nature of ferroelectricity and ferromagnetism [31]. Further, H. Murakawa et al demonstrated that the hybridization mechanism is the origin of the magnetoelectric response in $\text{Ba}_2\text{XGe}_2\text{O}_7$ (X = Mn, Co, and Cu) [32].



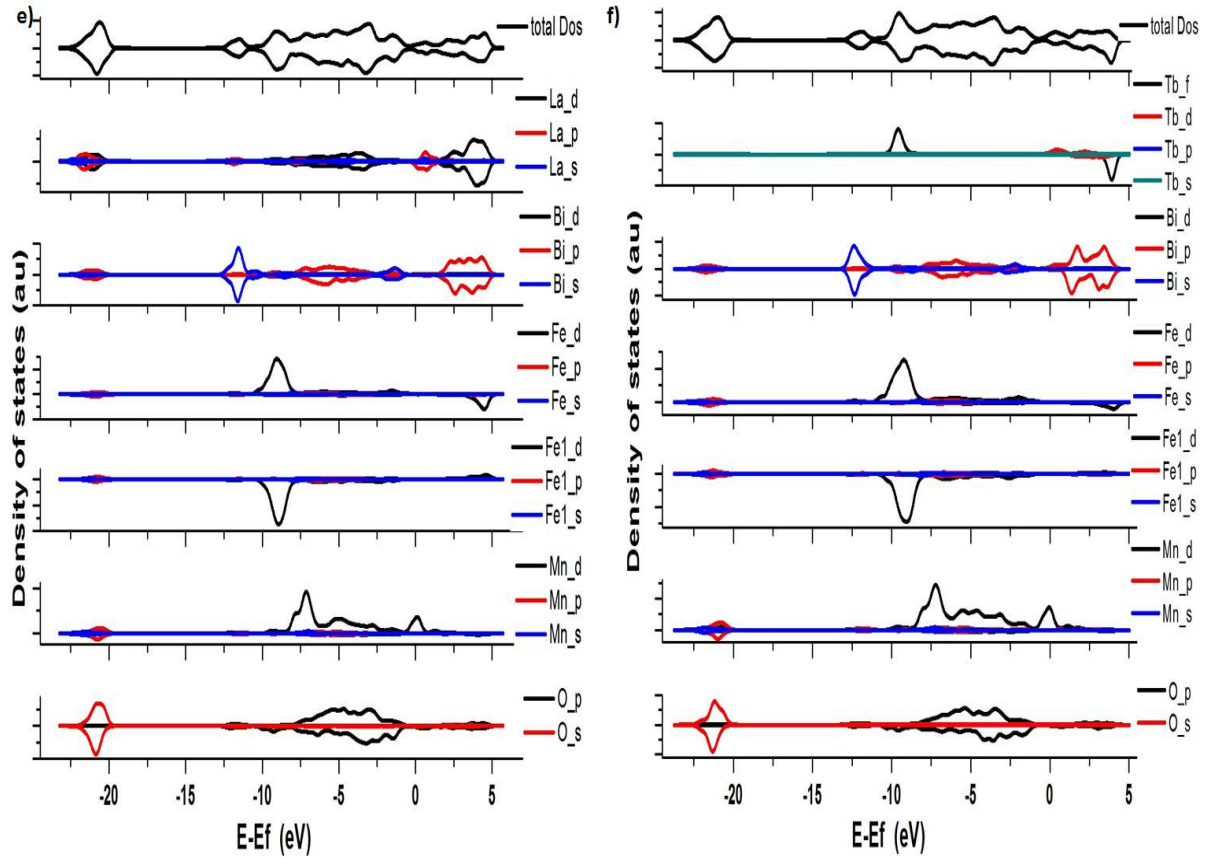


Figure.3: Total and partial densities of states of (a) BiFeO₃-ErMnO₃, (b) BiFeO₃-EuMnO₃, (c) BiFeO₃-GdMnO₃, (d) BiFeO₃-HoMnO₃, (e) BiFeO₃-LaMnO₃ and (f) BiFeO₃-TbMnO₃ compounds, the Fermi energy is set to be 0 eV.

The Fe-3d electrons in BiFeO₃ stay at high-spin configuration $t_{2g}^3 e_g^2$, (the valence of Fe ions is close to +3 (Fe³⁺)), and both of spin up and spin down states of Fe-3d are split by the octahedral crystal ligand field into t_{2g} and e_g orbitals [33]. **Figure.4** presents the spin up and spin down of Gd-d, Fe-3d and O-2p states, which are characterized by a strong overlapping of Gd-d, Fe-3d (e_g) and O-2p states between -7.5 eV and 0 eV, indicating the covalent feature for the Gd-O bonding and the hybridization between the Fe-3d and O-2p states decreases. As a result, Gd doping decreases the valence fluctuation of Fe ions, the remanent magnetization decreases and increases the local magnetic moment due to high magnetic moment of Gd, which is in good agreement with experimental study reported by Lahmar et al. [34], where the magnetization decreases with increasing the concentration of GdMnO₃. Also, a similar behavior was observed by M. Hasan et al [17] in Mn doping in Bi_{0.85}Gd_{0.15}Fe_{1-x}Mn_xO₃ system, which notes that the saturation magnetization rises gradually up to 10% Mn doping in Bi_{0.85}Gd_{0.15}Fe_{1-x}Mn_xO₃ system, whereas for a further increase of the Mn doping concentration decreases of the saturation magnetization. For instance, Hassan et

al.[17] reported that Gd^{3+} and Mn^{3+} co-doping BFO nanoparticle induced the suppression of spiral modulated spin structure that leads to improvement of the room temperature magnetization. The outstanding magnetic properties caused by this simultaneous presence in BFO thin films could be found also in earlier works of Lahmar et al.[18,19,34] where co-doping with the same concentration of Jahn-Teller active Mn^{3+} ions and RE-elements (other than Gd) reinforce the antiferromagnetic character of BFO, while the presence of Gd induces improvement of magnetization, governed by specific structural changes. In fact, Raman scattering measurements reveal that all vibration modes between 100 and 250 cm^{-1} of Bi–O bonds reduced with increasing the $GdMnO_3$ concentrations in BFO [34]. In meantime, a peak at around 300 cm^{-1} arises which is attributed tilting of oxygen octahedra [34]. It is worth mentioning that substituting Bi^{3+} with the much smaller Gd^{3+} ions produced local stresses in the lattice. The latter leads to make the motion of oxygen cages, suggesting the rotation of oxygen octahedra. Moreover, the local stress (octahedral distortion) results in changes in canting angle between Fe^{3+} ions could be the origins of magnetization improvement in $GdMnO_3$ doped BFO [34] (further discussion on local stress in the next paragraph).

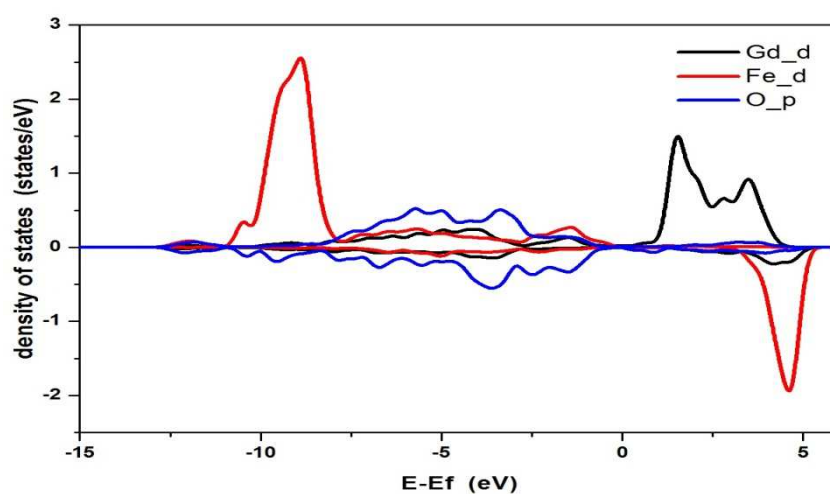


Figure.4. Partial densities of states of $BiFeO_3-GdMnO_3$ (Gd-d, Fe-3d and O-2p states), the Fermi energy is set to be 0 eV.

3.3 Jahn-Teller distortion:

Jahn-Teller distortion or Jahn-Teller effect was proposed in 1937, which removes the degeneracy of the e_g and t_g orbitals and undergoes distortion to form a system of lower symmetry and minimum of energy [35]. The electronic configuration of Mn in $BiFeO_3-GdMnO_3$ is $3d^4$, with the oxidation state of Mn^{3+} , giving a high-spin configuration for Mn^{3+} , which leads to the activation of the Jahn-Teller distortion [36]. There are two different

electronic configurations for Mn^{3+} ion: $(t_{2g})^3(dz^2)$ which induces two bonds along the z-axis direction and $(t_{2g})^3 d(x^2-y^2)$ which induces four bonds in the xy-plane. **Figure.5a** shows the calculated Mn–O and Fe–O bond lengths in $\text{BiFeO}_3\text{-GdMnO}_3$. The bond lengths of the Mn–O bonds in MnO_6 octahedron are 3.735 Å, 3.715 Å, 3.676 Å, 3.709 Å, 3.653 Å and 3.634 Å. While, the Fe–O bonds in FeO_6 octahedron are 3.749 Å, 3.782 Å, 3.706 Å, 3.733 Å, 3.727 Å and 3.688 Å. Comparing with FeO_6 octahedron, the O atoms move towards the Mn atom, indicating that a local distortion takes place around Mn^{3+} ions in $\text{BiFeO}_3\text{-GdMnO}_3$. The partial density of states of Mn-3d states, Mn-3d z^2 and Mn-3d(x^2-y^2) orbital of Mn atoms are shown in **Figure.5b**. Our calculations show that the distortion is not a strict Jahn-Teller distortion but is instead a preferential elongation of two of the Mn–O bonds (i.e., the pseudo Jahn-Teller distortion) due to the hybridization of the unoccupied 3d dxz and dx 2 -y 2 orbitals (see **Figure.5b**). Similar distortion of the Mn local environment has been observed by L. F. J. Piper et al [37] in Li_xMnPO_4 studied by soft and hard synchrotron-based spectroscopy with first-principles density functional theory within the GGA+U.

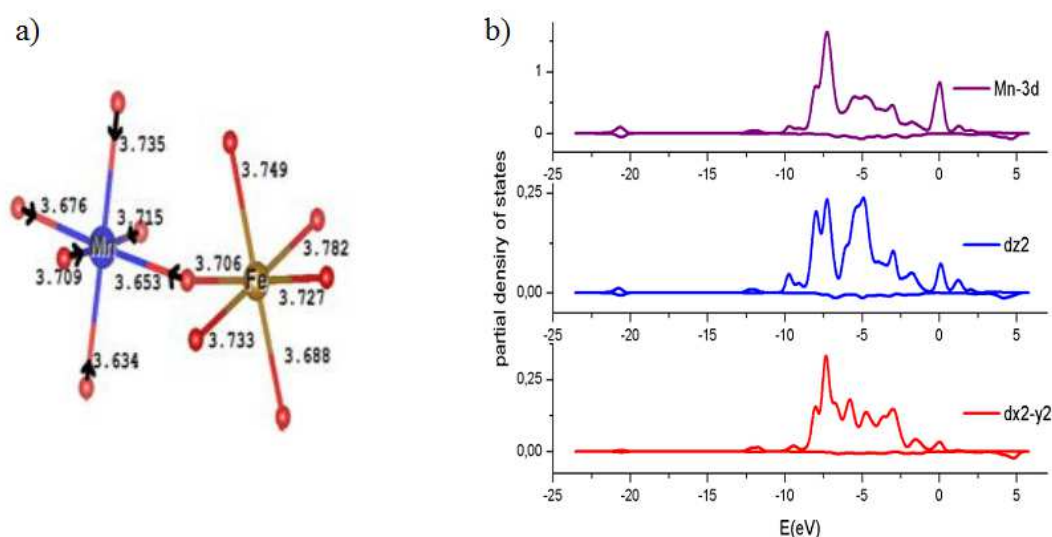


Figure.5: (a) pseudo Jahn–Teller distortion of the MnO_6 octahedron around of Mn in $\text{BiFeO}_3\text{-GdMnO}_3$, (b) the partial density of states of Mn-3d states, Mn-3d z^2 and Mn-3d(x^2-y^2) orbital of Mn atoms in $\text{BiFeO}_3\text{-GdMnO}_3$. The Fermi energy is set to be 0 eV.

Another important parameter describes the octahedral tilting angle (θ) between two adjacent octahedra, which are manifested by angles between different Fe–O–Fe and Fe–O–Mn bonds in these octahedra. The Fe–O–Fe and Mn–O–Fe bond angles between two adjacent octahedra in $\text{BiFeO}_3\text{-GdMnO}_3$ are shown in **Figure.6a**. We note that both Fe–O–Fe and Mn–O–Fe bond angles are lower than 180° and the tilting angle θ for Fe–O–Fe is lower than the Mn–O–Fe (from $\sim 152^\circ$ to $\sim 154^\circ$ in b-axis and from $\sim 150.92^\circ$ to $\sim 154.72^\circ$ in a-axis) in $\text{BiFeO}_3\text{-GdMnO}_3$.

GdMnO₃. The achieved values for Fe-O-Fe bond angle are very comparable to the experimental results of Bi_{0.85}Gd_{0.15}Fe_{0.9}Mn_{0.1}O₃ [17]. In addition, the O-Mn-O and O-Fe-O bond angles are 178.15° and 179.15°, respectively, which are lower than 180° (see **Figure.6b**). Also, the individual octahedron MnO₆/ FeO₆ shows that the individual O-Mn and Mn-O / O-Fe and Fe-O bond angles are not identical with 90° (see **Figure.6b**), indicating that the individual octahedron also contains distortions arising both from asymmetry in Mn-O bond lengths and bond angles. The changes in the tilting angle θ for Fe-O-Fe and Mn-O-Fe indicated a rotation of oxygen octahedra which can explain the origin of the peak at 300 cm⁻¹ observed in Raman measurements [18]. It is worth mentioning that the rhombohedral (R3c) to orthorhombic (Pn21a) phase transition is observed to increase with increasing Mn doping in Bi_{0.85}Gd_{0.15}Fe_{1-x}Mn_xO₃ and a pure orthorhombic phase is attained for x=0.15 [17-19]. Furthermore, the increasing of Gd/Mn doping in Bi_{1-y}Gd_yFe_{1-x}Mn_xO₃ produced the changes in Mn-O bond lengths and bond angles which leads to invoke local stresses in the system and arises the orthorhombic phase. Our calculations demonstrate that the distortion in GdMnO₃ doped BFO is the pseudo Jahn-Teller distortion with the changes in the octahedral tilting angle θ , as a mechanism responsible for higher magnetization and the Raman scattering measurements in GdMnO₃ doped BFO [17,34].

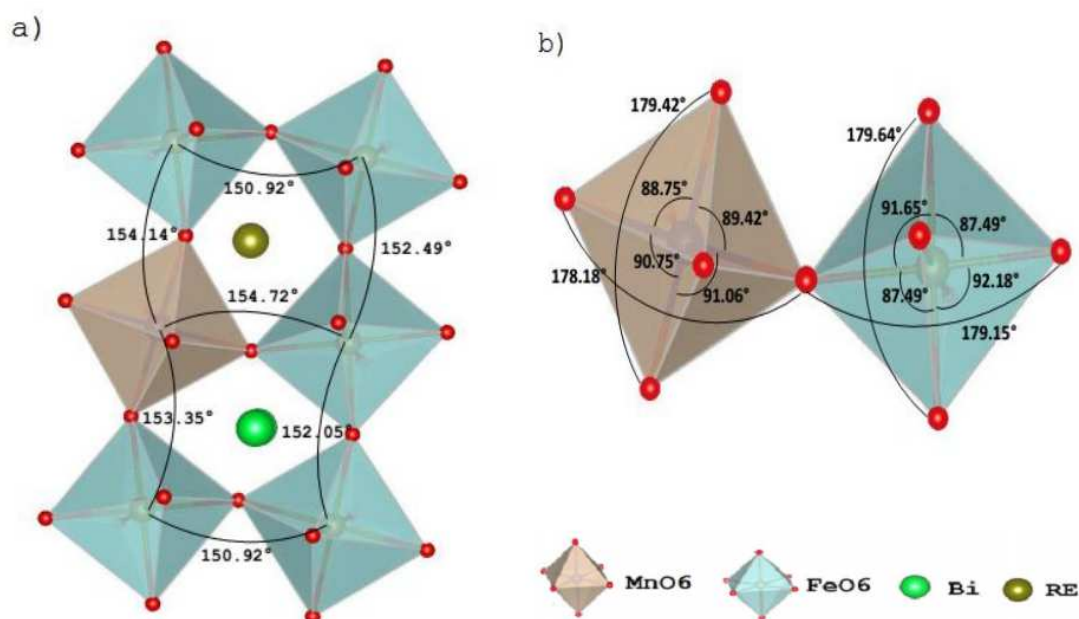


Figure.6: (a) Fe–O–Fe and Fe–O–Mn bond angles between two adjacent octahedra and (b) Mn–O and O–Fe bond angles in the individual octahedron in BiFeO₃-GdMnO₃

3.4 Spontaneous polarizations:

Spontaneous polarization was computed using first-principle calculations based on the Berry phase method [38]. The total polarization can be expressed as the sum of ionic polarization (P_{ion}) and electronic polarization (P_{el}) [39]. The Berry phase calculation yields a spontaneous polarization of 56.06, 60.84, 47.80, 62.02, 49.73 and $34.97 \mu\text{C}/\text{cm}^2$ in $\text{BiFeO}_3\text{-REMnO}_3$ for RE= Er, Eu, Gd, Ho, La and Tb, respectively, as shown in **Figure.7a**. Excellent agreement between the calculated spontaneous polarization and the experimental results reported by Lahmar et al [18,19]. In addition, Y. Han et al. [40] observed a similar improvement of ferroelectric property in $\text{Bi}_{0.8}\text{Er}_{0.2}\text{Fe}_{0.9}\text{Mn}_{0.1}\text{O}_3$, moreover, a giant 2Pr value of $231.4 \mu\text{C}/\text{cm}^2$ is observed in $\text{Bi}_{0.92}\text{Ho}_{0.08}\text{Fe}_{0.97}\text{Mn}_{0.03}\text{O}_3$ thin films by W. Ye et al [41]. The direction of spontaneous polarization in $\text{BiFeO}_3\text{-REMnO}_3$ depends on rare earth elements as shown in **Figure.7b**, where the direction of spontaneous polarization in $\text{BiFeO}_3\text{-REMnO}_3$ is [111] for RE= Er, Eu, Gd, Ho and Tb, while the direction of spontaneous polarization in $\text{BiFeO}_3\text{-LaMnO}_3$ is [101] and [001] for $\text{BiFeO}_3\text{-TbMnO}_3$.

Several works were demonstrated that REMnO_3 doped BiFeO_3 (or RE doped BiFeO_3) systems exhibit an enhancement of ferroelectric, ferromagnetic and electrochemical properties at concentration of 10% [42,46]. M. S. Bozgeyik et al [47] shows an improvement of saturation magnetization in $\text{Bi}_{0.9}\text{La}_{0.1}\text{Fe}_{0.9}\text{Gd}_{0.1}\text{O}_3$ (about four times) in comparison of $\text{Bi}_{0.9}\text{La}_{0.1}\text{FeO}_3$. A saturation magnetization of 2.20 emu/g was measured in $\text{Bi}_{0.85}\text{Gd}_{0.15}\text{Fe}_{0.9}\text{Mn}_{0.1}\text{O}_3$ with the coexistence of the both rhombohedral (R3c) and orthorhombic (Pn21a) phases [17]. Furthermore, the maximum of piezoelectric coefficient, remanent polarization and strain were obtained for $x = 0.10\text{--}0.12$ in $\text{Bi}_{1-x}\text{Sm}_x\text{Fe}_{0.99}\text{Ti}_{0.01}\text{O}_3$ thin films [48], the observed results were related to the coexistence of R3c and Pna21 phases (Morphotropic phase boundary: MPB) which leads to the sharp increase of these properties [49]. In the presented work, the density functional theory clarifies the properties of the bridging phase Pna21 which is the origin of high multiferroic properties in $\text{BiFeO}_3\text{-REMnO}_3$.

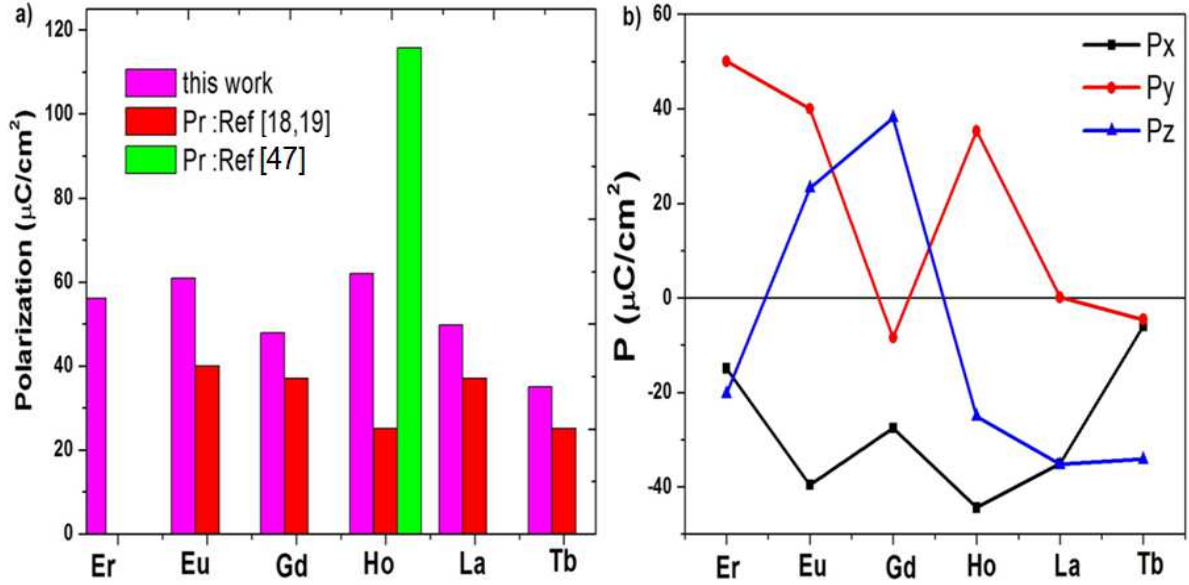


Figure.7: (a) Total spontaneous polarization with the experimental results reported in [18,19,39] and (b) its projection on (x, y, z) axis for $\text{BiFeO}_3\text{-REMnO}_3$ (RE = Er, Eu, Gd, Ho, La, Tb).

4. Conclusion:

First-principles in the framework of the density functional theory have been used to study the multiferroic properties of $\text{BiFeO}_3\text{-REMnO}_3$ (RE = Er, Eu, Gd, Ho, La, Tb). Our calculations achieved a total magnetic moment of 3.58, 4.69, 5.8, 4.27, 1.5 and 6.31 μ_B in $\text{BiFeO}_3\text{-REMnO}_3$ for RE= Er, Eu, Gd, Ho, La and Tb, respectively. In comparison with FeO_6 octahedron, the O atoms move towards the Mn atom, indicating that a local distortion takes place around of Mn^{3+} ions in $\text{BiFeO}_3\text{-GdMnO}_3$. Our calculations show that the distortion is not a strict Jahn-Teller distortion but is instead a preferential elongation of two of the Mn-O bonds (i.e., the pseudo Jahn -Teller distortion) due to the hybridization of the unoccupied 3d dxz and dx^2-y^2 orbitals. Measurements of the tilting angle θ for Fe-O-Fe are lower than that of the Mn-O-Fe (from $\sim 152^\circ$ to $\sim 154^\circ$ in b-axis and from $\sim 150.92^\circ$ to $\sim 154.72^\circ$ in a-axis) in $\text{BiFeO}_3\text{-GdMnO}_3$ which are lower than 180° . The Berry phase calculation yields a spontaneous polarization of 56.06, 60.84, 47.80, 62.02, 49.73 and 34.97 $\mu\text{C}/\text{cm}^2$ in $\text{BiFeO}_3\text{-REMnO}_3$ for RE= Er, Eu, Gd, Ho, La and Tb, respectively. These results are likely to offer useful information to the research communities' deal with BFO based multiferroic materials.

ACKNOWLEDGMENTS

ACKNOWLEDGMENTS

The authors are grateful to the financial support of this research by MESRSFC (Ministère de L'Enseignement Supérieur, de la Recherche Scientifique et de la Formation des Cadres) in the Framework of the national program PPR15/2015 and the European Union's Horizon 2020 research and innovation program ENGIMA.

Research Highlights

- BiFeO₃-REMnO₃ was investigated by First-principles.
- Pseudo Jahn–Teller distortion was predicted in BiFeO₃-GdMnO₃.
- Spontaneous polarization of BiFeO₃-REMnO₃ was determined by the berry phase method.

References:

- [1] J. Wang, J. B. Neaton, H. Zheng, V. Nagarajan, S. B. Ogale, B. Liu, D. Viehland, V. Vaithyanathan, D. G. Schlom, U. V. Waghmare, N. A. Spaldin, K. M. Rabe, M. Wuttig, R. Ramesh, *Science* 299(2003)1719–1722.
- [2] S.K. Singh, H. Ishiwara, K. Maruyama, *Appl.Phys.Lett.*88(2006)262908-4.
- [3] H.Naganuma and S. Okamura, *J. Appl. Phys.*, 2007, 101, 09M103.
- [4] H. Bea, M. Gajek, M. Bibes and A. Barthelemy, *J. Phys.: Condens. Matter*, 2008, 20, 434221.
- [5] D. S. Rana, I. Kawayama, K. Mavani and K. Takahashi, *Adv. Mater.*, 2009, 21, 2881.
- [6] L. W. Martin, S. P. Crane, Y.-H. Chu, M. B. Holcomb, M. Gajek, M. Huijben, C.-H. Yang, N. Balke, and R. Ramesh, *J. Phys. Condens. Matter* 20, 434220 (2008).
- [7] H. W. Jang, S. H. Baek, D. Ortiz, C. M. Folkman, R. R. Das, Y. H. Chu, P. Shafer, J. X. Zhang, S. Choudhury, V. Vaithyanathan, Y. B. Chen, D. A. Felker, M. D. Biegalski, M. S. Rzchowski, X. Q. Pan, D. G. Schlom, L. Q. Chen, R. Ramesh, and C. B. Eom, *Phys. Rev. Lett.* 101, 107602 (2008).
- [8] T. Zhao, A. Scholl, F. Zavaliche, K. Lee, M. Barry, A. Doran, M. P. Cruz, Y. H. Chu, C. Ederer, N. A. Spaldin, R. R. Das, D. M. Kim, S. H. Baek, C. B. Eom, and R. Ramesh, *Nat. Mater.* 5, 823 (2006).
- [9] F. Kubel and H. Schmid, *Acta Crystallogr., Sect. B: Struct. Sci.* 46, 698 (1990).
- [10] J. B. Neaton, C. Ederer, U. V. Waghmare, N. A. Spaldin and K. M. Rabe, *Phys. Rev. B: Condens. Matter*, 2005, 71, 014113.
- [11] P. Fischer, M. Polomska, I. Sosnowska, and M. Szymanski, *J. Phys. C* 13, 1931 (1980).
- [12] G. A. Smolenskii, V. Isupov, A. Agranovskaya, and N. Kranik, *Sov. Phys. Solid State* 2, 2651 (1961).
- [13] M.A. Basith, O. Kurni, M.S. Alam, B.L. Sinha, B. Ahmmad. *Journal of Applied Physics*, 115 (2014) 024102.
- [14] M.A. Basith, D.-T. Ngo, A. Quader, M.A. Rahman, B.L. Sinha, B. Ahmmad, F. Hirose, K. Mølhaveb . *Nanoscale*, 6 (2014) 14336-14342.

- [15] P. Tang, D. Kuang, S. Yang, Y. Zhang . *Journal of Alloys and Compounds*, 656 (2016) 912-919.
- [16] W. Zhou, H. Deng, H. Cao, J. He, J. Liu, P. Yang, J. Chu . *Materials Letters*, 144 (2015) 93-96.
- [17] Mehedi Hasan, M.A. Basith, M.A. Zubair, Md. Sarowar Hossain, Rubayyat Mahbub, M.A. Hakim, Md. Fakhrul Islam, *Journal of Alloys and Compounds*, Volume 687,2016, Pages 701-706, ISSN 0925-8388, <https://doi.org/10.1016/j.jallcom.2016.06.171>.
- [18] Abdelilah Lahmar, Mohammed Es-Souni. *Ceramics International* 41 (2015) 5721– 5726
- [19] A. Lahmar, S. Habouti, M. Dietze, C.-H. Solterbeck, and M. Es-Souni. *APPLIED PHYSICS LETTERS* 94, 012903 (2009).
- [20] W. Kohn, L. Sham, *Phys. Rev.* 140 (4A) (1965) A1133.
- [21] G. Kresse, J. Furthmüller, *Phys. Rev. B* 54 (1996) 11169.
- [22] X. Gonze et al., *Comput. Mater. Sci.* 25, 478 (2002)
- [23] L. Yin, W. Mi, X. Wang, *J. Mater. Chem. C*, 2015,3,11066-11075
- [24] D. Mekam, S. Kacimi, M. Djermouni, M. Azzouz, A. Zaoui. *Results in Physics* 2 (2512) 156–163
- [25] A. M. Rappe, K. M. Rabe, E. Kaxiras, and J. D. Joannopoulos, *Phys. Rev. B* 41, 1227 (1990).
- [26] <http://opium.sourceforge.net>
- [27] Ning Gao, Wei Chen, Ren Zhang , Jian Zhang, Zhenli Wu, Weiwei Mao, Jianping Yang, Xing'ao Li , Wei Huang. *Computational and Theoretical Chemistry* 1084 (2016) 36–42.
- [28] Wei Ye, Guoqiang Tann, Guohua Dong, Huijun Ren, Ao Xia. *Ceramics International* 41 (2015) 4668– 4674.
- [29] Yumin Han, Weiwei Mao, Chuye Quan, Xingfu Wang, Jianping Yang, Tao Yang ,Xing'ao Li, Wei Huang. *Materials Science and Engineering B* 188 (2014) 26–30.
- [30] Y.M. Han, W.W. Mao, C.Y. Quan, X.F. Wang, J.P. Yang, T. Yang, X.A. Li, W. Huang, Enhancement of magnetic and ferroelectric properties of BiFeO₃ by Er and transition element (Mn, Co) co-doping, *Mater. Sci. Eng. B* 188 (2014) 26–30.
- [31] Cai M Q, Liu J C, Yang G W, Cao Y L, Tan X, Chen X Y, Wang Y G, Wang L L and Hu W Y 2007 First-principles study of structural, electronic, and multiferroic properties in BiCoO₃ *J. Chem. Phys.* 126 154708
- [32] H. Murakawa, Y. Onose, S. Miyahara, N. Furukawa, and Y. Tokura. *PHYSICAL REVIEW B* 85, 174106 (2012)
- [33] M. Abbate, F. De Groot, J. Fuggle, A. Fujimori, O. Strebler, F. Lopez, M. Domke, G. Kaindl, G. Sawatzky, M. Takano, *Physical Review B* 46 (8) (1992) 4511.
- [34] A. Lahmar, S. Habouti, C-H. Solterbeck, M. Dietze, and M. Es-Souni. *JOURNAL OF APPLIED PHYSICS* 107, 024104 2010 .
- [35] H.A. Jahn, E. Teller, *Proc. R. Soc.* 161 (1937) 220.
- [36] J. D. Dunitz and L. E. Orgel, *J. Phys. Chem. Solid.* , 1957, 3, 20-29.
- [37] L. F. J. Piper, N. F. Quackenbush, S. Sallis, D. O. Scanlon, G. W. Watson, K.-W. Nam, X.-Q. Yang, K. E. Smith, F. Omenya, N. A. Chernova, and M. S. Whittingham. [dx.doi.org/10.1021/jp3122374](https://doi.org/10.1021/jp3122374). *J. Phys. Chem.*
- [38] R.D. King-Smith, D. Vanderbilt, *Phys. Rev. B* 47 (1993) 1651.
- [39] Qiaoqiao Zhang, Qun Jing, Haiming Duan, Haibin Cao. *Journal of Solid State Chemistry*. <https://doi.org/10.1016/j.jssc.2018.04.031>
- [40] Yumin Han, Weiwei Mao, Chuye Quan, Xingfu Wang, Jianping Yang b, Tao Yang, Xing'ao Li, Wei Huang. *Materials Science and Engineering B* 188 (2014) 26–30.

- [41] Wei Ye, Guoqiang Tann, Guohua Dong, Huijun Ren, Ao Xia. *Ceramics International* 41 (2015) 4668– 4674.
- [42] T. Wang, X.-L. Wang, S.-H. Song, Q. Ma, Effect of rare-earth Nd/Sm doping on the structural and multiferroic properties of BiFeO₃ ceramics prepared by spark plasma sintering, *Ceramics International*. 46 (2020) 15228–15235. <https://doi.org/10.1016/j.ceramint.2020.03.061>.
- [43] F. Mumtaz, S. Nasir, G.H. Jaffari, S.I. Shah, Chemical pressure exerted by rare earth substitution in BiFeO₃: Effect on crystal symmetry, band structure and magnetism, *Journal of Alloys and Compounds*. 876 (2021) 160178. <https://doi.org/10.1016/j.jallcom.2021.160178>.
- [44] C.-S. Chen, C.-S. Tu, W.S. Chang, Y.H. Huang, P.-Y. Chen, Y.-T. Lee, Improved polarization switching and piezoresponse in Nd and Mn co-doped BiFeO₃ ceramics, *Materials Science and Engineering: B*. 269 (2021) 115180. <https://doi.org/10.1016/j.mseb.2021.115180>.
- [45] L.T. Mai Oanh, D.V. Thang, D.D. Bich, P.D. Chung, N.M. Hung, N. Van Quang, N. Van Minh, Enhancement of ferroelectric and ferromagnetic properties of Gadolinium (Gd) and Nickel (Ni) co-doped BiFeO₃, *Ceramics International*. 46 (2020) 17423–17429. <https://doi.org/10.1016/j.ceramint.2020.04.036>.
- [46] S. Sharma, H.A. Reshi, J.M. Siqueiros, O. Raymond Herrera, Stability of rhombohedral structure and improved dielectric and ferroelectric properties of Ba, Na, Ti doped BiFeO₃ solid solutions, *Ceramics International*. (2021). <https://doi.org/10.1016/j.ceramint.2021.09.261>.
- [47] M.S. Bozgeyik et al., Monitoring structural variation on Gd ratio of La modified bismuth ferrite ceramics with enhanced magnetization, *Journal of Alloys and Compounds*, <https://doi.org/10.1016/j.jallcom.2019.153050>
- [48] Xin Xin Shi, Xiao Qiang Liu, and Xiang Ming Chen. *Journal of Applied Physics* 119, 064104 (2016); doi: 10.1063/1.4941820
- [49] P. Mandal, A. Manj on-Sanz, A. J. Corkett, T. P. Comyn, K. Dawson, T. Stevenson, J. Bennett, L. F. Henrichs, A. J. Bel, E. Nishibori, M. Takata, M. Zanella, M. R. Dolgos, U. Adem, X. M. Wan, M. J. Pitcher, S. Romani, T. T. Tran, P. S. Halasyamani, J. B. Claridge, and M. J. Rosseinsky, *Adv. Mater.* 27, 2883 (2015).

